Available online at www.sciencedirect.com
SCIENCE DIRECT
Journal of Catalysis 235 (2005) 393–402
JOURNAL OF CATALYSIS
www.elsevier.com/locate/jcat

# Supporting monolayer Pt on W(110) and C/W(110): Modification effects on the reaction pathways of cyclohexene

M.B. Zellner [a], J.G. Chen [b,*]

[a] Department of Materials Science and Engineering, Center for Catalytic Science and Technology (CCST), University of Delaware, Newark, DE 19716, USA
[b] Department of Chemical Engineering, Center for Catalytic Science and Technology (CCST), University of Delaware, Newark, DE 19716, USA

Received 11 April 2005; revised 2 September 2005; accepted 6 September 2005

**Abstract**

The decomposition, dehydrogenation, self-hydrogenation, and hydrogenation of cyclohexene were used as probe reactions to determine the effects of supporting monolayer Pt on W(110) and C/W(110) surfaces. The reaction pathways were studied using temperature-programmed desorption (TPD) and high-resolution electron energy loss spectroscopy (HREELS). On the clean and carbon-modified W(110) surfaces, the dominant reaction pathway of cyclohexene is the complete decomposition to produce hydrogen and atomic carbon. Monolayer Pt-modification of the W(110) and C/W(110) surfaces reduces the complete decomposition and enhances the selectivity toward the dehydrogenation of cyclohexene to produce gas phase benzene. More importantly, unlike previous studies of supporting monolayer Pt on Ni and Co surfaces, neither self-hydrogenation of cyclohexene nor hydrogenation of cyclohexene with coadsorbed hydrogen is detected on the monolayer Pt-modified W(110) and C/W(110) surfaces. The comparison is consistent with our previous density functional theory (DFT) modeling of monolayer Pt on different substrates, confirming that the chemical properties of supported Pt vary significantly on different substrates.


*Keywords:* W(110); C/W(110); Pt; Cyclohexene; Bimetallics; TPD; HREELS

## 1. Introduction

The formation of bimetallic alloys or metal carbides offers the possibility of tuning the electronic properties of transition metals, leading to bimetallic or carbide catalysts with catalytic activity and selectivity that differ from those of the parent metals. Various chemical, electronic, and physical probes have been used to understand activity and selectivity modifications at an atomic level [1–9]. Progress in computational technology has also made it feasible to use theoretical calculations to facilitate understanding at a fundamental level [10–13]. Regarding the novel properties of bimetallic surfaces, Goodman and coworkers demonstrated a strong correlation between the desorption temperature of CO and the core electron energy shift in bimetallic surfaces [3–5]. Similarly, alloying carbon atoms with early transition metals has proven to be another way of tuning the surface electronic and chemical properties [14–16].

One very useful probe molecule for characterizing the reactivity of bimetallic and carbide surfaces is cyclohexene (c-$C_6H_{10}$), which can undergo several types of reactions, including complete decomposition to produce atomic carbon and hydrogen, dehydrogenation to produce benzene and hydrogen, and self-hydrogenation (disproportionation reaction) to produce cyclohexane. These reactions provide information regarding the cleavage of the C–C bond, as well as the scission and formation of the C–H bond. For example, on early transition metal surfaces such as W(111) and W(110), cyclohexene undergoes complete decomposition [17,18]. On Pt-group metal surfaces, such as Pt(111), cyclohexene undergoes both complete decomposition and dehydrogenation to produce benzene [18–21]. Finally, on bimetallic surfaces, such as monolayer Ni/Pt(111), Pt/Ni(111), and Co/Pt(111), a fraction of cyclohexene also undergoes self-hydrogenation to produce cyclohexane [22–25].

* Corresponding author.
*E-mail address:* jgchen@udel.edu (J.G. Chen).

0021-9517/$ – see front matter 
doi:10.1016/j.jcat.2005.09.007

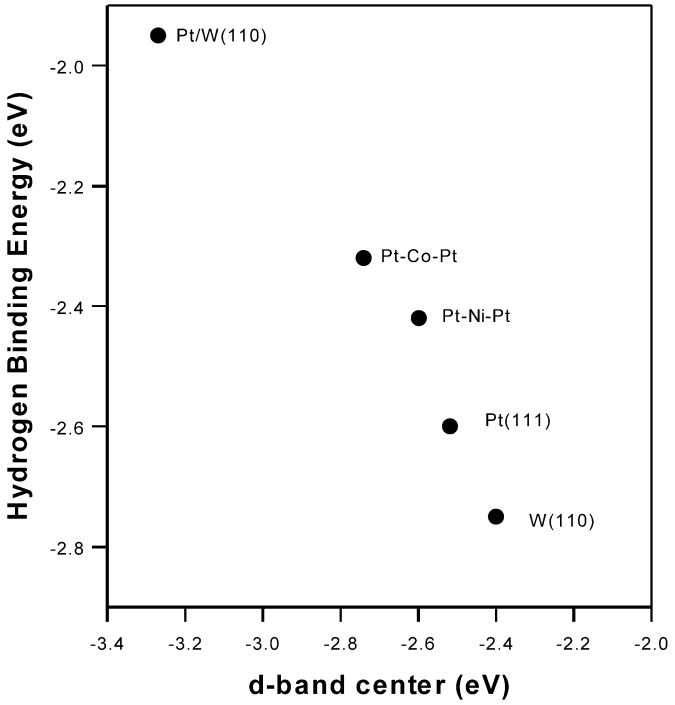


Fig. 1. DFT calculated hydrogen binding energy plotted verse d-band center for various metals and bimetallic surfaces [12,24].

The goal of the current work is to compare the reaction pathways of cyclohexene on Pt/W(110), C/W(110), and Pt/C/W(110) to determine the effect of bimetallic and carbide formation on the reactivity of W(110). In particular, the choice of Pt/W(110) as the model bimetallic surface is based on our recent experimental investigation and DFT modeling of different bimetallic surfaces [10–13]. For example, Fig. 1 compares the DFT modeling results for W(110), Pt(111), and monolayer Pt on W(110), which have been reported previously [11–13]. The DFT results show that the d-band center of the Pt/W(110) surface is shifted away from the Fermi level compared with that of either W(110) or Pt(111). The shift in the d-band center in turn reduces the binding energy of hydrogen on Pt/W(110) compared with that on either parent metal. For comparison, Fig. 1 also includes the d-band center and hydrogen binding energy of two other Pt-containing bimetallic surfaces, Pt–Co–Pt(111) and Pt–Ni–Pt(111), which can be experimentally prepared by the diffusion of one monolayer Co [22] or Ni [5,10] into the subsurface region of Pt(111), respectively. Compared with Pt(111), the Pt–Co–Pt(111) and Pt–Ni–Pt(111) surfaces show a reduced hydrogen binding energy, which have been confirmed experimentally [5,22]. In addition, the presence of more weakly bonded hydrogen on the Pt–Co–Pt(111) and Pt–Ni–Pt(111) surfaces also promotes the self-hydrogenation and hydrogenation of cyclohexene, which do not occur on clean Pt(111). Based on the trend shown in Fig. 1, one might expect the Pt/W(110) surface to be even more active for the self-hydrogenation and hydrogenation of cyclohexene if one assumes that the hydrogenation activity is related to the strength of hydrogen binding energy. As we demonstrate in the current study on Pt/W(110), such a simple correlation is not necessarily valid.

In the current study we also use the C/W(110) surface to further investigate the possible correlation between the hydrogen binding energy and hydrogenation activity. Recent DFT results on carbides have suggested that, similar to bimetallic systems, the formation of metal carbides also leads to a shift in the d-band center [11,19,26]. For example, we recently compared the surface d-band center and hydrogen binding energy on Mo(110) and C/Mo(110) and found that the formation of carbide on Mo(110) resulted in a shift of the d-band center away from the Fermi level and a corresponding reduction in hydrogen binding energy. Considering the general similarity between the Mo(110) and W(110) surfaces, one would expect the formation of carbide on W(110) to also lead to a reduction in hydrogen binding energy. Therefore, a comparative study of hydrogenation of cyclohexene on W(110) and C/W(110) should reveal whether the hydrogenation activity is related to the hydrogen binding energy.

The current study also compares the effect of supporting monolayer Pt on C/W(110) to determine whether the Pt/C/W(110) surface exhibits unique activities, such as the synergistic effects observed earlier on Pt/C/W(111) toward the reactions of cyclohexene [27] and methanol [28]. Overall, the comparison of monolayer Pt on W(110) and C/W(110) with previous studies of supported Pt on other substrates should provide insight into how the chemical properties of monolayer Pt films are modified by the interaction with different substrates.

Supported Pt catalysts are among the most commonly used heterogeneous catalysts in various commercial processes. In this paper we provide direct evidence that the hydrogenation activity of Pt depends strongly on the interaction with the substrates. In addition, combining the results from the current paper with our previous results on supported Pt on other metal substrates, we illustrate the possibility of tuning the hydrogenation activity of Pt by the formation of Pt-based bimetallic catalysts. Finally, our results clearly indicate a volcano-type relationship between the strength of the metal–hydrogen bond and the hydrogenation activities. This fundamental understanding on well-characterized model surfaces should provide useful input for the rational design and synthesis of supported Pt catalysts with desirable hydrogenation activities.

The current study uses temperature-programmed desorption (TPD) and high-resolution electron energy loss spectroscopy (HREELS) to investigate reaction pathways of cyclohexene on W(110), Pt/W(110), and Pt/C/W(110) surfaces. We first report TPD results of cyclohexene and of coadsorption of cyclohexene and hydrogen on clean and modified W(110) and C/W(110) surfaces. We then present HREELS results of surface intermediates after the reaction of cyclohexene. Finally, we compare these results with the trends in the literature for various bimetallic and carbide surfaces.

## 2. Experimental

### 2.1. Techniques

The ultrahigh-vacuum (UHV) chamber has been described in detail previously [28]. Briefly, it is a three-level stainless-

steel chamber (base pressure of $3 \times 10^{-10}$ Torr) equipped with Auger electron spectroscopy (AES) and TPD in the top two levels and HREELS in the bottom level. The TPD experimental setup allowed us to monitor up to 12 masses simultaneously. The spectra were recorded with the opening of the random flux shield of the quadrupole mass spectrometer placed at a distance of ∼5 mm from the sample surface. The HREELS spectra reported here were acquired with a primary beam energy of 6 eV. Angles of incidence and reflection were 60° with respect to the surface normal in the specular direction. Count rates in the elastic peak were typically in the range of $5 \times 10^5$–$2 \times 10^6$ counts per second (cps), and the spectral resolution was between 35 and 50 $cm^{-1}$ FWHM (full-width at half-maximum).

The tungsten single-crystal sample was a [110]-oriented, 1.5-mm-thick, 8-mm-diameter tungsten disk (99.999% purity; Metal Crystals and Oxides, Ltd., Cambridge, UK). The crystal was spot-welded directly to two tantalum posts that served as electrical connections for resistive heating, as well as thermal contacts for cooling with liquid nitrogen. With this mounting scheme, the temperature of the crystals could be varied between 100 and 1300 K.

Cyclohexene (99+% purity; Aldrich) was purified by successive freeze-pump-thaw cycles before use. The purity was verified in situ by mass spectrometry. In all experiments, gas exposures were made with the substrate at approximately 100 K and with the surface in front of the leak valve. The gas exposures were made by backfilling the chamber. Doses are reported in Langmuirs [1.0 Langmuir (L) = $1 \times 10^{-6}$ Torr s] and are uncorrected for ion gauge sensitivity.

### 2.2. Preparation of clean and modified W(110) surface

Preparation of the clean W(110) surface has been described in detail previously [29]. Briefly, the W(110) crystal was cleaned using multiple cycles of $Ne^+$ sputtering while held at 600 K, followed by annealing to 1200 K. To remove extra carbon species, the crystal was exposed to 10 L of oxygen at 1200 K. This cleaning procedure was repeated until negligible C or O signals were detected by AES. The C/W(110) surface was prepared by exposing W(110) to ethylene at 100 K and then flashed to 1200 K; generally, these procedures were repeated for three cycles, and produced a C/W(110) surface with an Auger C(KLL 272 eV)/W(MNN 182 eV) peak ratio between 0.5 and 0.7, corresponding to an atomic C/W ratio between 0.54 and 0.75 using standard AES sensitivity factors.

Pt-modified W(110) surfaces were prepared using physical vapor deposition (PVD) of Pt with the W(110) and C/W(110) surfaces held at 600 K. The evaporative PVD doser consisted of a tungsten filament with a high-purity (99.9999+%) Pt wire wrapped around it, mounted on a stainless-steel enclosure. The Pt coverage was estimated from the reduction of the AES W(MNN 182 eV) intensity before and after Pt deposition, based on the assumption that uniform Pt overlayers are deposited. This assumption was observed in earlier studies of Madey et al. [30] that confirmed layer-by-layer growth of Pt on W(110).

## 3. Results

### 3.1. TPD results

Fig. 2 shows the TPD spectra of hydrogen from modified W(110) surfaces after a 50-L exposure of $H_2$. On the clean W(110) surface, the major hydrogen desorption peak occurred at 405 K. On the C/W(110) surface, the desorption occurred as a very broad peak between 143 and 405 K, with a noticeable feature at 265 K. On the 1.0 ML Pt/W(110) and 1.0 ML Pt/C/W(110) surfaces, hydrogen desorption occurred as a single feature at 143 K with a broad tail.

Figs. 3a–d show the TPD spectra of cyclohexene, hydrogen, benzene, and cyclohexane, respectively, from modified W(110) surfaces after a 2-L exposure of cyclohexene. On the clean W(110) surface, cyclohexene desorption occurred at 226 K with an asymmetric shoulder at 183 K. Hydrogen desorption occurred as a broad feature centered at 411 K, whereas benzene desorption occurred as a relatively sharp feature centered at 315 K. On the C/W(110) surface, cyclohexene desorbed at 183 K with an asymmetric shoulder at 252 K. Hydrogen desorption occurred as two peaks centered at 280 and 411 K and benzene desorbed at 315 K. A very weak cyclohexane desorption peak was also detected at 260 K. On the 1.0 ML Pt/W(110) surface, cyclohexene desorbed at 183 K, with a second slightly

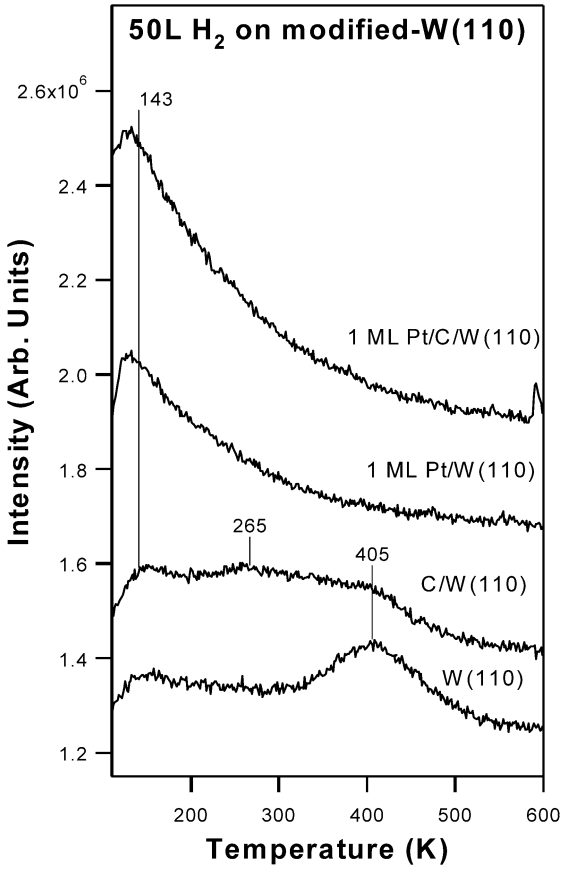


Fig. 2. Temperature-programmed desorption spectra of $H_2$ following the adsorption of 50 L $H_2$ on clean and modified W(110) surfaces.

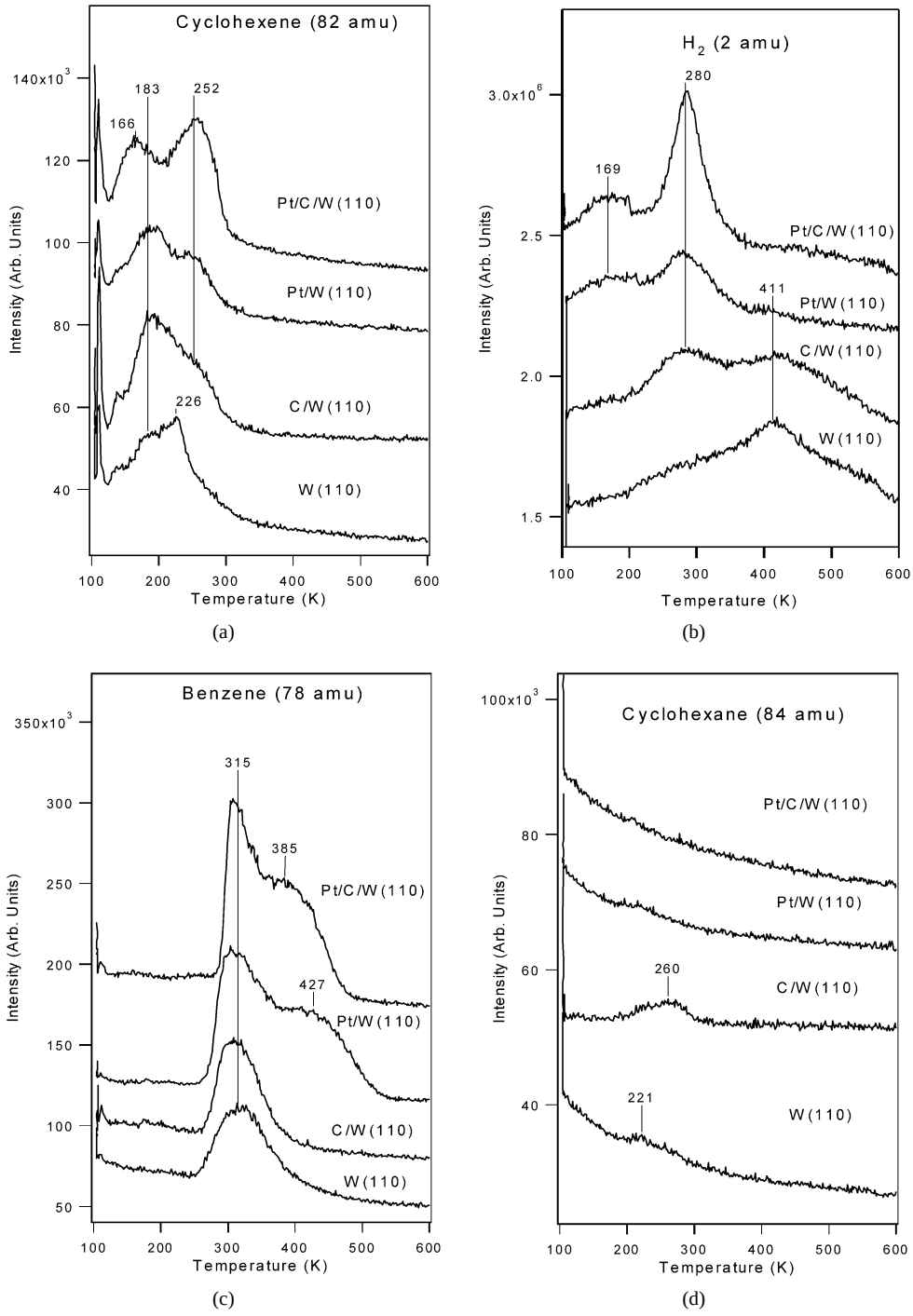


Fig. 3. Temperature-programmed desorption spectra of (a) c-$C_6H_{10}$, (b) $H_2$, (c) $C_6H_{10}$, and (d) c-$C_6H_{12}$ following the reactions of 2 L exposure of c-$C_6H_{10}$ on clean and modified W(110) surfaces.

weaker feature at 252 K. Hydrogen desorption occurred at 280 K and as a relatively weak and broad feature at 169 K. The desorption of the benzene product occurred at 315 K, with a second feature at 427 K. Finally, on the 1.0 ML Pt/C/W(110) surface, cyclohexene desorbed as two peaks at 166 and 252 K. Hydrogen desorbed as a relatively sharp peak centered at 280 K, and benzene desorbed at 315 K with a large shoulder at 385 K.

Figs. 4a–d show the gas-phase desorption products from preadsorption of 2 L hydrogen followed by 2 L of cyclohexene on modified W(110) surfaces. On the clean W(110) surface, cyclohexene desorbed as three peaks at 162, 207, and 232 K, with an asymmetric shoulder at ∼265 K. Hydrogen desorption was detected at 148 and 260 K, and benzene desorbed at 305 and 420 K. A relatively weak cyclohexane desorption was detected as a single peak at 191 K. On the C/W(110) surface, cyclohexene desorbed as a broad feature that ranged from 160 to 230 K, and hydrogen desorbed at 273 K with a second, weaker desorption feature at 148 K. Benzene desorbed from the sur-

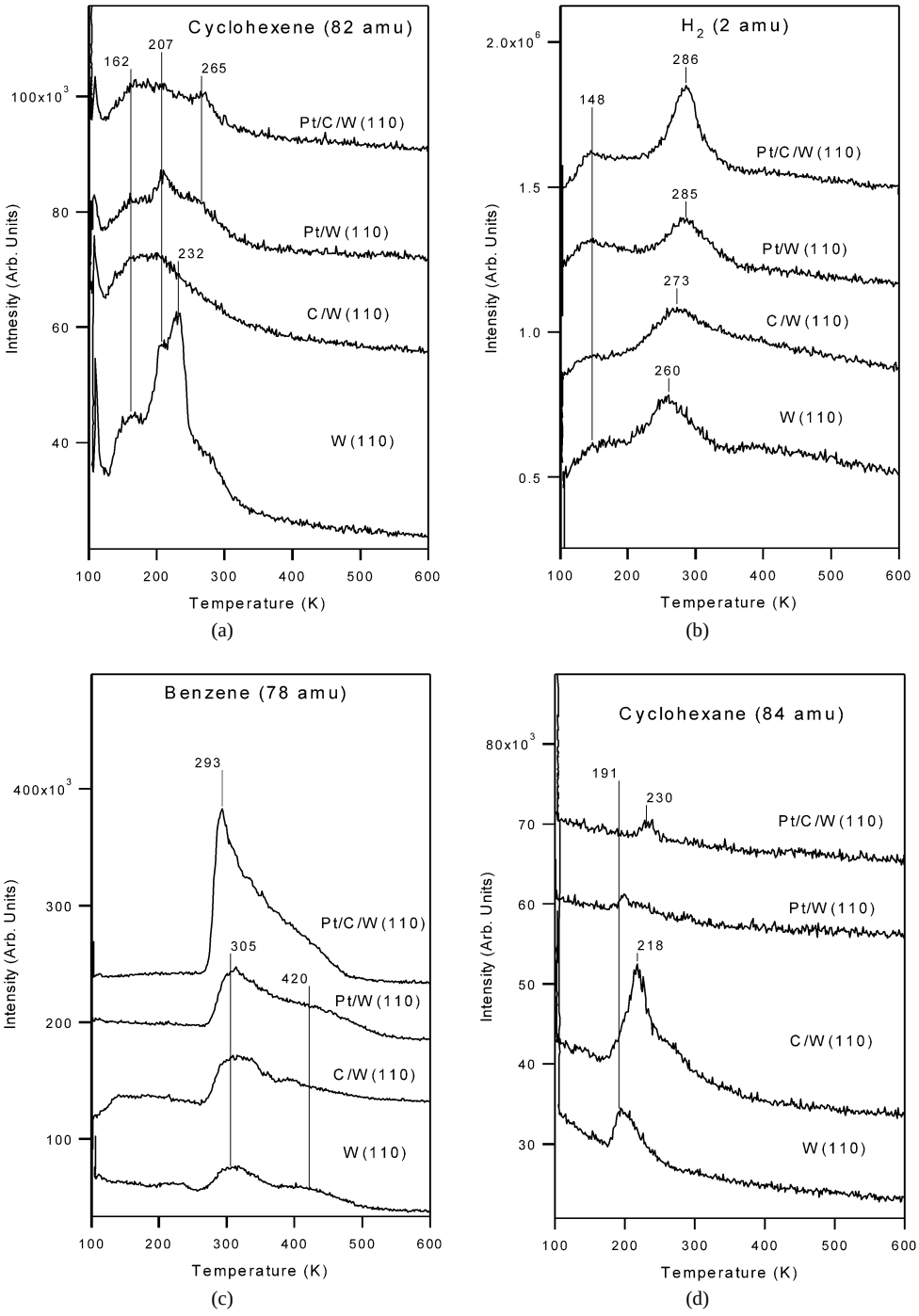


Fig. 4. Temperature-programmed desorption spectra of (a) c-$C_6H_{10}$, (b) $H_2$, (c) $C_6H_{10}$, and (d) c-$C_6H_{12}$ following the coadsorption of 2 L $H_2$ and 2 L c-$C_6H_{10}$ on clean and modified W(110) surfaces.

face at 305 K, and cyclohexane desorbed from the surface as a relatively sharp feature centered at 218 K, with a shoulder at ∼250 K. On the ML Pt/W(110) surface, cyclohexene desorbed at 207 K, with shoulders at 162 and 265 K. Hydrogen desorption occurred at 148 and 285 K, whereas benzene desorbed at 305 K, with a second weaker desorption peak at 420 K. On the 1.0 ML Pt/C/W(110) surface, cyclohexene desorbed as a broad peak ranging from ∼130 to 270 K. Hydrogen desorption occurred at 148 and 286 K, whereas benzene desorbed at 293 K with a large tail.

### 3.2. HREELS results

This section describes the HREEL spectra after the thermal decomposition of adsorbed c-$C_6H_{10}$ on various surfaces. The exposures of cyclohexene were made with the crystal temperature at 100 K; then the adsorbed layer was heated to the indicated temperatures and cooled immediately before each HREEL spectrum was recorded. Finally, the height of the elastic peaks in all spectra were normalized to unity, and the expan-

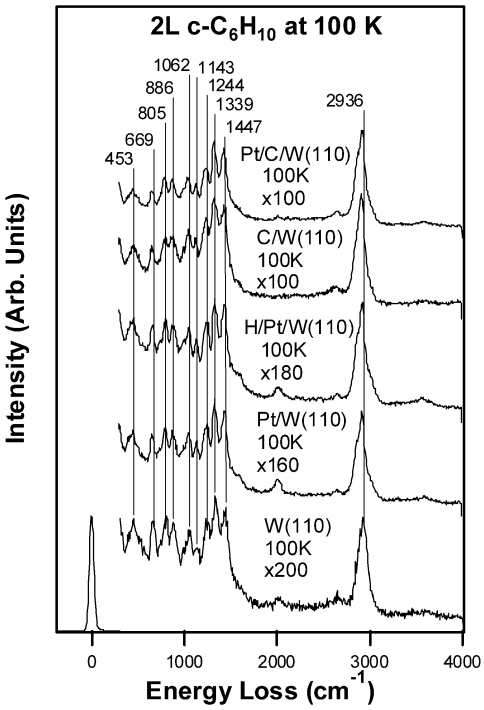


Fig. 5. HREEL spectra after adsorption of 2 L c-$C_6H_{10}$ on various surfaces at 100 K.

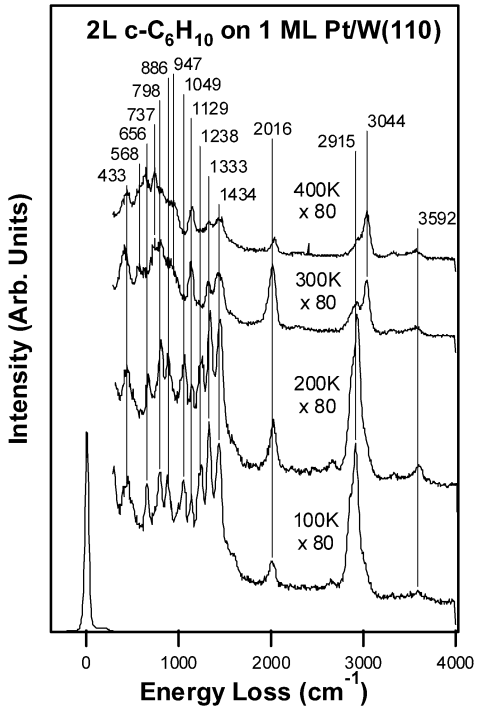


Fig. 6. HREEL spectra monitoring the thermal decomposition of 2 L c-$C_6H_{10}$ on 1.0 ML Pt/W(110).

Table 1
Vibrational assignments for cyclohexene on modified W(110) surfaces at 100 K

| Mode | Liquid | W(110) | C/W(110) | 1.0 ML Pt/W(110) | 1.0 ML Pt/C/W(110) |
|---|---|---|---|---|---|
| Ring deformation | 452 | 453 | 453 | 433 | 440 |
| Skeletal distortion | 640, 670 | 669 | 669 | 656 | 656 |
| $\delta$(C=C) | 720 | | | | |
| $\nu$(C–C) | 810 | 805 | 805 | 798 | 791 |
| $\nu$(C–C) | 905, 917 | 886 | 886 | 886 | 879 |
| $\nu$(C–C) & $\rho(CH_2)$ | 1038 | 1062 | 1062 | 1049 | 1049 |
| $\omega CH_2$ (rock) | 1138 | 1143 | 1143 | 1129 | 1123 |
| $\omega CH_2$ (wag) | 1241, 1264 | 1244 | 1244 | 1238 | 1231 |
| $\omega CH_2$ (twist) | 1321–1350 | 1339 | 1339 | 1333 | 1326 |
| $\delta CH_2$ (scissors) | 1438–1456 | 1447 | 1447 | 1434 | 1434 |
| $\nu$(C=C) | 1653 | | | | |
| $\nu$(–C–H) | 2840–2993 | 2936 | 2936 | 2915 | 2916 |
| $\nu$(=C–H) | 3026, 3065 | | | | |

sion factor for each individual spectrum represents the multiplication factor relative to the elastic peak.

Fig. 5 shows HREEL spectra after the adsorption of 2 L of c-$C_6H_{10}$ at 100 K on various surfaces. Vibrational assignments of features on W(110) and C/W(110) surfaces are summarized in Table 1. The following vibrational features were identified: 453 $cm^{-1}$, ring deformation; 669 $cm^{-1}$, skeletal distortion; 805 $cm^{-1}$, $\nu$(C–C); 886 $cm^{-1}$, $\nu$(C–C); 1062 $cm^{-1}$, $\nu$(C–C), and $\rho(CH_2)$; 1143 $cm^{-1}$, $\omega(CH_2)$ rock; 1244 $cm^{-1}$, $\omega(CH_2)$ wag; 1339 $cm^{-1}$, $\omega(CH_2)$ twist; 1447 $cm^{-1}$, $\delta(CH_2)$ scissors; 2936 $cm^{-1}$, $\nu$(–C–H). The absence of a $\nu$(C=C) at ~1600 $cm^{-1}$ indicates that the cyclohexene intermediates are strongly bound to both the clean and carbon-modified surfaces at 100 K. More details about the HREELS study after the decomposition of cyclohexane have been described previously [17]. Briefly, thermal decomposition results from previous work show that the cyclohexene intermediate remained stable on the surface to temperatures up to 300 K, followed by decomposition at higher temperatures.

Fig. 5 also compares the HREELS spectra after the adsorption of 3 L of cyclohexene on 1.0 ML of Pt/W(110), both with and without the preadsorption of hydrogen, and on 1.0 ML of Pt/C/W(110). In general, the vibrational features on these surfaces at 100 K are very similar to those assigned on W(110) and are summarized in Table 1. Additional vibrational features at 2016 and 3592 $cm^{-1}$ are attributed to the accumulation of CO and $H_2O$ from the UHV background during acquisition (~40 min/spectrum). The absence of the $\nu$(C=C) vibrational mode at ~1600 $cm^{-1}$ indicates that at 100 K, cyclohexene is strongly bound to the Pt-modified surfaces.

Fig. 6 shows HREEL spectra after the thermal decomposition of 2 L of cyclohexene on the 1-ML Pt/W(110) surface. Heating to 200 K produced no significant spectroscopic changes. Heating to 300 K resulted in the following spectroscopic changes: (1) a reduction in intensity and broadening of vibrational features related to the strongly bound cyclohexene intermediate; (2) the appearance of the $\gamma$(C–H) vibrational mode of benzene at 737 $cm^{-1}$; and (3) a partial shift of the $\nu$(–C–H) vibrational feature at 2915 $cm^{-1}$ to the dehydrogenated $\nu$(=C–H) vibrational feature at 3044 $cm^{-1}$. Further heating to 400 K resulted in a slight reduction in intensity of all intermediates, accompanied by the onset of a $\nu$(metal–C) vibrational mode at 656 $cm^{-1}$. HREELS studies after the thermal decomposition of cyclohexene on the H/Pt/W(110) and Pt/C/W(110) surfaces revealed similar spectroscopic changes (spectra not shown).

## 4. Discussion

### 4.1. Activity and product selectivity

On the W(110), C/W(110), Pt/W(110), and Pt/C/W(110) surfaces, hydrogen, benzene, and cyclohexene were the gas phase products, and atomic carbon was the remaining surface species after heating the surface to 600 K. The reaction pathways on the surfaces are as follows:

$$x\text{c-}C_6H_{10} \xrightarrow{\Delta} 6x\text{C(a)} + 5xH_2\text{(g)}, \quad (1)$$

$$y\text{c-}C_6H_{10} \xrightarrow{\Delta} yC_6H_6\text{(g)} + 2yH_2\text{(g)}, \quad (2)$$

$$z\text{c-}C_6H_{10} + 2H \xrightarrow{\Delta} z\text{c-}C_6H_{12}\text{(g)}. \quad (3)$$

The values of $x$, $y$, and $z$ represent the amounts of cyclohexene molecules undergoing different reaction pathways. The value of $x$ in Eq. (1) and $y$ in Eq. (2) have been previously determined on W(110), using a combination of TPD and AES [17], to be $x = 0.073$ and $y = 0.0013$ $C_6H_{10}$ per surface W atom, respectively. To estimate the benzene product yield [value of $y$ from Eq. (2)] on the C/W(110), 1.0 ML Pt/W(110), and 1.0 ML Pt/C/W(110) surfaces, the following relationship based on the benzene TPD peak area can be used

$$\frac{y_{W(110)}}{y_{Surface}} = \frac{\text{area}^{W(110)}_{Benzene}}{\text{area}^{Surface}_{Benzene}}. \quad (4)$$

Evaluation of Eq. (4) using 0.0013 for $y_{W(110)}$ and the corresponding benzene TPD peak area on various surfaces leads to $y = 0.0015$ for the C/W(110) surface, 0.0041 for the 1.0 ML Pt/W(110) surface, and 0.0038 for the 1.0 ML Pt/C/W(110) surface.

The activity for cyclohexene self-hydrogenation on the W(110) and C/W(110) surfaces was estimated by comparing the peak areas of benzene and cyclohexane, normalized by the relative mass spectrometer sensitivity, as shown in Eq. (5). The relative mass spectrometer sensitivity for cyclohexane (84 amu) and benzene (78 amu) was determined previously as follows [22]. By taking into consideration of the different ion gauge sensitivities for c-$C_6H_{12}$ (6.4) and $C_6H_6$ (5.9), and by exposing the UHV chamber to equal pressures of c-$C_6H_{12}$ ($6.4 \times 10^{-8}$ Torr) and $C_6H_6$ ($5.9 \times 10^{-8}$ Torr), the mass spectrometer intensity ratio was determined to be 0.41 for c-$C_6H_{12}$/$C_6H_6$:

$$\frac{y_{Surface}}{z_{Surface}} = \frac{\text{area}^{Surface}_{Benzene}}{\text{area}^{Surface}_{Cyclohexane}} \times 0.41. \quad (5)$$

Evaluation of Eq. (5) using 0.0013 for $y_{W(110)}$, 0.0015 for $y_{C/W(110)}$, and the corresponding peak areas of cyclohexane resulted in $z_{W(110)} < 0.0001$ and $z_{C/W(110)} = 0.0002$ cyclohexane molecules per surface W atom.

As shown in the reaction pathways in Eqs. (1)–(3), the TPD hydrogen peak areas are affected by three reactions. In the complete decomposition [Eq. (1)], each cyclohexene molecule undergoes complete decomposition to produce 5 hydrogen molecules. In the dehydrogenation pathway [Eq. (2)], each cyclohexene molecule produces 2 hydrogen molecules. Finally, in the self-hydrogen pathway [Eq. (3)], 1 hydrogen molecule (2 hydrogen atoms) is consumed for the hydrogenation of each cyclohexene molecule. To estimate the activity toward the complete decomposition [value of $x$ from Eq. (1)] on the various surfaces, the following relationship based on the hydrogen TPD peak area can be used

$$\frac{5x_{W(110)} + 2y_{W(110)} - z_{W(110)}}{5x_{Surface} + 2y_{Surface} - z_{Surface}} = \frac{\text{area}^{W(110)}_{Hydrogen}}{\text{area}^{Surface}_{Hydrogen}}. \quad (6)$$

Evaluation of Eq. (6) using 0.073 for $x_{W(110)}$, 0.0013 for $y_{W(110)}$, 0.0001 for $z_{W(110)}$, the corresponding calculated value for $y_{Surface}$, and the corresponding measured hydrogen TPD peak area, the value of $x$ is estimated as 0.062 for the C/W(110) surface, 0.032 for the 1.0 ML Pt/W(110) surface, and 0.042 for the 1.0 ML Pt/C/W(110) surface.

Based on these values, the total activity toward the decomposition of $C_6H_{10}$ molecules per metal site were estimated to be $x + y + z = 0.074$ for W(110), $x + y + z = 0.064$ for C/W(110), $x + y = 0.036$ for 1.0 ML Pt/W(110), and $x + y = 0.046$ for 1.0 ML Pt/C/W(110). These results are summarized in Table 2 and compared with the values from similar cyclohexene coverage on a Pt(111) surface. The typical errors bars for the values reported in Table 2, based on the analysis of multiple TPD measurements on W(110) and C/W(110), are within 10% of the corresponding values.

To quantify the effect of preadsorbed hydrogen on the dehydrogenation and hydrogenation pathways, the product yields of benzene and cyclohexane are estimated from the TPD peak areas in Fig. 3. The pathway for complete decomposition is not quantified, because of the contribution of preadsorbed hydrogen to the total hydrogen TPD peak areas. These results are summarized in Table 3 and compared with previous results from the hydrogenation of cyclohexene with preadsorbed hydrogen on the monolayer Pt/Ni(111), Pt–Ni–Pt(111), and Pt–Co–Pt(111) surfaces.

Table 2
Activity and selectivity of cyclohexene on various surfaces

| Surface | Complete decomposition | Dehydrogenation to benzene | Self-hydrogenation to cyclohexane | Overall reactivity cyclohexene | Selectivity to benzene (%) |
|---|---|---|---|---|---|
| W(110) [17] | 0.073 | 0.0013 | <0.0001 | 0.074 | 2 |
| C/W(110) | 0.062 | 0.0015 | 0.0002 | 0.064 | 2 |
| 1.0 ML Pt/W(110) | 0.032 | 0.0041 | 0 | 0.036 | 11 |
| 1.0 ML Pt/C/W(110) | 0.042 | 0.0038 | 0 | 0.046 | 8 |
| Pt(111) [19] | 0.09 | 0.03 | 0 | 0.12 | 25 |

Table 3
Effect of preadsorbed hydrogen on product selectivity (molecules/metal atom)

| | $C_6H_6$ product | c-$C_6H_{12}$ product |
|---|---|---|
| W(110) | 0.001 | 0.0002 |
| C/W(110) | 0.001 | 0.0006 |
| 1.0 ML Pt/W(110) | 0.002 | < 0.0001 |
| 1.0 ML Pt/C/W(110) | 0.004 | < 0.0001 |
| Pt–Ni–Pt | 0.024 | 0.006 |
| Pt–Co–P [22] | 0.026 | 0.006 |
| 1.0 ML Pt/Ni(111) [23] | 0.016 | 0.040 |

### 4.2. Comparison of W(110), C/W(110), Pt/W(110), and Pt/C/W(110)

As summarized in Table 2, on clean W(110), cyclohexene undergoes primarily two reaction pathways: (1) complete decomposition (98%) to form gas phase hydrogen and atomic carbon or (2) dehydrogenation (2%) to form gas phase benzene and hydrogen. The reaction pathways on the C/W(110) surface are very similar, with a slight reduction in the overall activity from 0.074 cyclohexene molecules undergoing reaction on clean W(110) to 0.064 cyclohexene molecules. Another difference is that the self-hydrogenation pathway is more noticeable on C/W(110) than on W(110), although the yield of the cyclohexane product is negligibly small from both surfaces.

On the 1.0 ML Pt/W(110) and 1.0 ML Pt/C/W(110) surfaces, cyclohexene also undergoes both complete decomposition and dehydrogenation, although the presence of monolayer Pt modifies the overall activity and product selectivity. As shown in Table 2, the presence of Pt leads to a reduction in the complete decomposition pathway, which is accompanied by an increase in the yield and selectivity of the dehydrogenation reaction pathway to produce gas phase benzene. HREEL spectra of cyclohexene exposed to the 1.0 ML Pt/W(110) (Fig. 6) and 1.0 ML Pt/C/W(110) (not shown) surfaces reveal partial dehydrogenation to form surface-bonded benzene intermediates by 300 K. TPD spectra (Fig. 3c) also confirm the enhanced dehydrogenation pathway by the onset of a new benzene desorption peak at >315 K and by the increase in the overall desorption peak area of benzene. The TPD spectra in Fig. 3 also reveal minor differences between the Pt/W(110) and Pt/C/W(110) surfaces, as indicated by the different benzene desorption temperatures and different peak areas of the hydrogen product on the two surfaces. Furthermore, as shown in Table 2, the activity and product selectivity of the two monolayer Pt surfaces are significantly different from those of bulk Pt(111).

The most important observation for the ML Pt/W(110) and Pt/C/W(110) surfaces is the absence of any self-hydrogenation pathway to produce cyclohexane. The TPD results in Fig. 4 also show that cyclohexane is not produced on these two surfaces after the coadsorption of 2 L of cyclohexene and 2 L of hydrogen. In fact, comparing the peak areas of cyclohexane in Fig. 4d, it appears that the presence of monolayer Pt on W(110) and C/W(110) inhibits the hydrogenation pathway that is noticeable on unmodified W(110) and C/W(110) surfaces. The absence of the self-hydrogenation and hydrogenation pathways on the monolayer Pt surfaces is significantly different from previous studies on other substrates, as discussed below.

### 4.3. Comparison with Pt monolayer films on other substrates

As shown in the DFT modeling in Fig. 1, the hydrogen binding energy (HBE) decreases as the center of the surface d-band shifts away from the Fermi level. This trend has been confirmed previously in the TPD experiments on ML Pt–Ni–Pt(111), Pt–Co–Pt(111), and Pt/Ni(111) [22,23,25]. In those experiments, the desorption temperature of $H_2$, which is related to HBE assuming that the dissociation of $H_2$ is an unactivated process, occurs at ∼200 K. This temperature is much lower than the desorption temperature from either Ni(111) or Pt(111), qualitatively confirming the DFT results. In addition, the DFT modeling also suggests that the value of HBE would be further decreased for the Pt/W(110) surface. This is consistent with the TPD results in Fig. 2, which show that the desorption temperature of $H_2$ occurs at ∼148 K, significantly lower than that from either W(110) (405 K) or Pt(111) (∼300 K) [19]. In addition, the desorption temperature of $H_2$ from the C/W(110) surface occurs at lower temperatures than from clean W(110), consistent with the DFT modeling showing that the formation of carbide leads to a shift away from the Fermi level.

Overall, the comparison in Figs. 1 and 2 confirm a similar trend between DFT modeling and TPD experiments regarding the HBE on different bimetallic surfaces. However, the hydrogenation activity does not follow the same trend. Reactions of cyclohexene on monolayer Ni/Pt(111), Ni/W(110), and Co/Pt(111) bimetallic systems have been shown to undergo self-hydrogenation to produce cyclohexane [22,23], which does not occur on Pt(111) or on thick Ni and Co surfaces. In all cases, self-hydrogenation to produce gas phase cyclohexane occurs as a relatively sharp TPD peak between 200 and 220 K. In addition, coadsorption of cyclohexene with hydrogen enhances the yield of cyclohexene on all surfaces, as summarized in Table 3. However, on 1.0 ML Pt/W(110), TPD spectra (Figs. 4b and d) show that the Pt/W(110) bimetallic surface does not follow this trend. No gas phase cyclohexane is detected from either the self-hydrogenation of cyclohexene or the hydrogenation of cyclohexene coadsorbed with hydrogen. In addition, on the C/W(110) surface, coadsorption of hydrogen and cyclohexene produced small amounts of the hydrogenated cyclohexane product (Fig. 4d). Monolayer Pt-modification of the C/W(110) surface inhibits this reaction, eliminating the hydrogenation pathway on the 1.0 ML Pt/C/W(110) surface.

The absence of the self-hydrogenation and hydrogenation pathways on ML Pt/W(110) could be due to two factors. The first of these is related to the weak HBE on Pt/W(110). As shown in Fig. 2, The desorption of hydrogen from Pt/W(110) occurs at approximately 140 K, which is 60–80 K lower than that from the Pt/Ni(111), Pt–Ni–Pt(111), and Pt–Co–Pt(111) surfaces [22,23,25]. The self-hydrogenation and hydrogenation of cyclohexene on the latter surfaces occur at 200–240 K. This would suggest that, due to the very low desorption temperature of hydrogen from Pt/W(110), atomic hydrogen likely is no longer available at the temperature necessary for the self-

hydrogenation and hydrogenation of cyclohexene. This hypothesis can be tested by performing similar studies on different Pt–M–Pt(111) surfaces, where M represents a monolayer of 3d metal located between the first and second layers of Pt(111). As predicted from DFT modeling, the HBE gradually decreases as the 3d metal moves from late transition metals (e.g., Ni, Co) to early transition metals (e.g., Ti, V). An investigation of self-hydrogenation and hydrogenation on Pt–Ti–Pt(111) should provide further insight into the relationship between HBE and the hydrogenation activity of Pt-based bimetallic surfaces.

The second explanation is that the monolayer Pt might undergo morphology change on the adsorption of cyclohexene. This is suggested by the detection of the di-$\sigma$ bonded cyclohexene on the ML Pt/W(110) surface in the HREELS measurements. This observation differs from our previous studies of the adsorption of cyclohexene on ML Pt/Ni(111) and Pt–Ni–Pt(111) surfaces, where the adsorption of cyclohexene occurred primarily via the weakly $\pi$-bonded configuration. These results allowed us to suggest that the onset of the low-temperature hydrogenation pathway was due to the presence of both weakly adsorbed hydrogen and cyclohexene. The observation of di-$\sigma$ bonded cyclohexene in the current study might be due to the clustering of the Pt atoms, leaving exposed W atoms to form the strongly bonded di-$\sigma$ species and thus preventing the self-hydrogenation and hydrogenation pathways. It is important to point out that the ML Pt/W(110) surface appears to be stable on the adsorption of hydrogen, as indicated by the absence of an $H_2$ desorption peak from the clean W(110) substrate based on the desorption temperatures. More detailed studies using scanning tunneling microscopy (STM) or low-energy ion scattering (LEIS) are needed to determine whether the adsorption of cyclohexene causes the change in the morphology of the ML Pt/W(110) surface.

Despite the uncertainty about the origins for the absence of the hydrogenation pathway on Pt/W(110), our results indicate that the correlation between HBE and hydrogenation activity does not follow a simple linear relationship of various Pt-based bimetallic surfaces. Our results also reveal that the hydrogenation activity of monolayer Pt depends strongly on the nature of the substrates, which offers the possibility of controlling the hydrogenation activity of supported Pt by using different substrates and forming different bimetallic alloys.

It should be pointed out that the primary interest in supporting Pt on W and C/W in the current study is to produce Pt-based bimetallic surfaces, and to use these surfaces as model systems to further illustrate that the chemical properties of Pt can be tuned by choosing different alloy components. In practice, it would be difficult to use W or C/W as catalyst supports, because of issues related to their stability and low surface areas. However, it should be possible to support Pt and W (or Pt and C/W) on high-surface area supports, such as alumina or silica, to produce the corresponding high-surface area bimetallic catalysts.

Finally, as described in our recent papers after the batch reactor studies on supported Ni/Pt [31] and Co/Pt [32] bimetallic catalysts, there is a strong correlation between the hydrogenation activities on model surfaces and supported catalysts. For example, we observe that both the Co/Pt(111) model surface and the supported Co/Pt/$\gamma$-$Al_2O_3$ catalyst show enhanced low-temperature hydrogenation activity compared with the corresponding monometallic surfaces and catalysts. Results from parallel DFT modeling [12] indicate that the preferred structure of the Co/Pt(111) surface, at a monolayer coverage, is the Pt–Co–Pt(111) structure with the monolayer Co occupying between the first and second layers of Pt. This Pt–Co–Pt "sandwich" structure is stable under reducing conditions, such as in vacuum and in a hydrogen environment [12]. Because both the bimetallic Co/Pt(111) and supported Co/Pt catalysts are prepared under reducing conditions, the model surface and supported catalyst are likely both characterized with Co atoms occupying the subsurface sites underneath the first layer of Pt, leading to the very good agreement in reactivity between model surfaces and supported catalysts. Reactor studies are currently underway on supported Pt/W catalysts to further test the correlation between model surfaces and the corresponding supported catalysts.

## 5. Conclusions

From the results and discussion presented above, the following conclusions can be made regarding the reaction pathways of cyclohexene on the Pt/W(110), C/W(110), and Pt/C/W(110) surfaces:

1. The dominant reaction pathways of cyclohexene on the clean W(110) and C/W(110) surfaces is the complete decomposition to atomic carbon and gas phase hydrogen (98%). The minor reaction pathway on the two surfaces is dehydrogenation to produce gas phase benzene and hydrogen (2%). The self-hydrogenation pathway is negligible on both surfaces.
2. The 1.0 ML Pt/W(110) surface promotes the dehydrogenation of cyclohexene to produce gas phase benzene, with the selectivity increasing from 2 to 11% on Pt/W(110). The presence of Pt also reduces the overall activity of W(110), with the amount of cyclohexene decreasing from 0.074 to 0.036 molecules per metal atom.
3. Compared with C/W(110), the presence of monolayer Pt enhances the dehydrogenation pathway slightly, with the selectivity increasing from 2 to 8%. The presence of Pt also reduces the number of cyclohexene undergoing reaction from 0.064 on C/W(110) to 0.046 on Pt/C/W(110).
4. The self-hydrogenation of cyclohexene or the hydrogenation of coadsorbed hydrogen and cyclohexene does not occur on the 1.0 ML Pt/W(110) surface. This observation differs from previous studies of monolayer Pt films on other surfaces, such as Pt/Ni(111), Pt–Ni–Pt(111), and Pt–Co–Pt(111). These comparisons suggest the possibility of tuning the chemical properties of supporting Pt by choosing different substrates.

## Acknowledgments

We acknowledge financial support from the Basic Energy Sciences division of the Department of Energy (DOE/BES Grant No. DE-FG02-00ER15014). MBZ acknowledges partial financial support from a National Aeronautics and Space Administration Fellowship grant (NGT5-40024).

## References

[1] J. Rodriguez, Surf. Sci. Rep. 24 (1996) 223–287.
[2] P.J. Berlowitz, D.W. Goodman, Surf. Sci. 187 (1987) 463.
[3] P.J. Berlowitz, J.E. Houston, J.M. White, D. Wayne Goodman, Surf. Sci. 205 (1988) 1–11.
[4] D.W. Goodman, Ultramicroscopy 34 (1990) 1–9.
[5] H.H. Hwu, J. Eng, J.G. Chen, J. Amer. Chem. Soc. 124 (2002) 702–709.
[6] N.A. Khan, H.H. Hwu, J.G. Chen, J. Catal. 205 (2002) 259–265.
[7] N.A. Khan, J.G. Chen, J. Phys. Chem. B 107 (2003) 4334–4341.
[8] J.H. Sinfelt, Bimetallic Catalysts, New York, Wiley, 1983.
[9] M.B. Zellner, A.M. Goda, O. Skoplyak, M.A. Barteau, J.G. Chen, Surf. Sci. 583 (2005) 281.
[10] J.R. Kitchin, N.A. Khan, M.A. Barteau, J.G. Chen, B. Yakshinskiy, T.E. Madey, Surf. Sci. 544 (2003) 295–308.
[11] J.R. Kitchin, J.K. Norskov, M.A. Barteau, J.G. Chen, Catal. Today 105 (2005) 66.
[12] J.R. Kitchin, J.K. Norskov, M.A. Barteau, J.G. Chen, Phys. Rev. Lett. 93 (2004) 1–4.
[13] J.R. Kitchin, J.K. Norskov, M.A. Barteau, J.G. Chen, J. Chem. Phys. 120 (2004) 10240–10246.
[14] J.G. Chen, Chem. Rev. 96 (1996) 1477–1498.
[15] S.T. Oyama, The Chemistry of Transition Metal Carbides and Nitrides, Glasgow, Blackie Academic and Professional, 1996.
[16] H.H. Hwu, J.G. Chen, Chem. Rev. 105 (2005) 185.
[17] B.D. Polizzotti, H.H. Hwu, J.G. Chen, Surf. Sci. 520 (2002) 97–110.
[18] N. Liu, S.A. Rykov, H.H. Hwu, M.T. Buelow, J.G. Chen, J. Phys. Chem. B 105 (2001) 3894–3902.
[19] J.A. Rodriguez, C.T. Campbell, J. Catal. 115 (1989) 500.
[20] D.P. Land, W. Erley, H. Ibach, Surf. Sci. 289 (1993) 237.
[21] F.C. Henn, A.L. Diaz, M.E. Bussell, M.B. Hugenschmidt, M.E. Domagala, C.T. Campbell, J. Phys. Chem. 96 (1992) 5965.
[22] N.A. Khan, L.E. Murillo, J.G. Chen, J. Phys. Chem. B 108 (2004) 15748–15754.
[23] N.A. Khan, M.B. Zellner, J.G. Chen, Surf. Sci. 556 (2004) 87–100.
[24] N.A. Khan, J.G. Chen, J. Vacuum Sci. Technol. A 21 (2003) 1302–1306.
[25] N.A. Khan, M.B. Zellner, L.E. Murillo, J.G. Chen, Catal. Lett. 95 (2004) 1–6.
[26] P. Liu, J.A. Rodriguez, Catal. Lett. 91 (2003) 247.
[27] N. Liu, J.G. Chen, Catal. Lett. 77 (2001) 35–40.
[28] N. Liu, K. Kourtakis, J.C. Figueroa, J.G. Chen, J. Catal. 215 (2003) 254–263.
[29] H.H. Hwu, J.G. Chen, J. Phys. Chem. B 107 (2003) 2029–2039.
[30] T.E. Madey, K.-J. Song, C.-Z. Dong, R.A. Demmin, Surf. Sci. 247 (1991) 175–187.
[31] N.A. Khan, J.R. Kitchin, V. Schwartz, L.E. Murillo, K.M. Bulanin, J.G. Chen, in: B. Zhou, S. Hermans, G.A. Somorjai (Eds.), Nanotechnology in Catalysis, vol. 1, Kluwer Academic/Plenum, New York, 2003, pp. 17–32.
[32] N.A. Khan, L.E. Murillo, Y. Shu, J.G. Chen, Catal. Lett. (2005), in press.